Insight - Civil Engineering 2024, 7(1), 613.
https://doi.org/10.18282/ice.v7i1.613

Article

Discovering the optimal distance between spatial orthogonal tunnels: A dynamic analysis using Tehran metro as a case study

Mehrdad Mohammadifar*, Tohid Asheghi Mehmandari, Seyed Ali Mirjafari

Civil and Environmental Engineering Faculty, Amirkabir University of Technology (Tehran Polytechnic), Tehran 1591634311, Iran

*** Corresponding author:** Mehrdad Mohammadifar, mmohammadifar@aut.ac.ir

CITATION

Mohammadifar M, Asheghi Mehmandari T, Mirjafari SA. Discovering the optimal distance between spatial orthogonal tunnels: A dynamic analysis using Tehran metro as a case study. Insight - Civil Engineering. 2024; 7(1): 613. https://doi.org/10.18282/ice.v7i1.613

ARTICLE INFO

Received: 28 April 2024
Accepted: 4 June 2024
Available online: 15 August 2024

Abstract: This study investigates the dynamic behavior of spatially orthogonal tunnels by employing three-dimensional numerical modeling and analyzing four different placement scenarios to determine the optimal tunnel spacing for minimizing mutual interaction while ensuring operational efficiency. This comprehensive research fills a vital gap in dynamic tunnel interaction studies and provides valuable insights for tunnel engineering in urban environments. Furthermore, in this research, the influence and response of adjacent shield tunnels under seismic conditions was evaluated based on the Tabas earthquake spectrum. Moreover, to enhance the accuracy of assumptions and achieve more logical results, the study utilizes the assumptions of the intersection tunnels of lines 6 and 7 of the Tehran metro. Dynamic analyses reveal that closer tunnel proximity (<0.5r) leads to increased bending moments, axial forces and displacements due to stress field interference, underscoring the critical importance of proper tunnel placement. Furthermore, results of the internal forces and displacements in both adjacent tunnels under dynamic loading show that positioning scenario case 2 (distance of tunnels is equal to their radius) is the most suitable option. In this scenario (compared to scenario case 1), the tunnels are less affected by each other's stress field, and also in this positioning scenario (compared to scenarios 3 and 4), access from the ground surface to the lower tunnel will be easier and with lower construction costs.

Keywords: spatially orthogonal tunnels; numerical modelling; intersection tunnels; earthquake

1. Introduction

The construction of a tunnel in close proximity to another tunnel will undoubtedly induce alterations in the stress distribution within the tunnel region. The alterations in the stress field are contingent upon multiple factors, including soil properties surrounding the tunnels, mechanical characteristics and thickness of the tunnels lining, spacing between the tunnels, shape and cross-sectional area of the tunnels, method employed for tunnel excavation, overburden on the tunnels and finally the tunnels' intersect angel.

The development of urban tunnels, particularly within metro networks, requires meticulous deliberation. Given the broad nature of underground metro lines and their frequent junctions with other lines at multiple stations along their routes, it is imperative to conduct a comprehensive examination of the interaction and impact of tunnels on one another. The necessity of this assessment is applicable in both static and dynamic states. Due to multiple reasons affecting on interaction of intersecting tunnels, design and implementation of these tunnels are challenging and risky. Furthermore, placement of these tunnels in urban areas increases the significance of

this issue. Therefore, it's crucial to have broad investigations before tunnel excavation [1,2].

Kim initiated investigations into the subject of intersecting tunnels and studied the interaction between closely spaced tunnels during shield tunnel construction, concentrating on the study of the short-term incremental behaviour of the liner. Also, a controlled physical model tests were carried out and the test results were complemented by a limited amount of numerical analysis [3]. A series of small-scale (1/50) laboratory model tests (conducted at 1 g) was carried out in Speswhite kaolin clay. These tests have been conducted to gain a greater understanding of the short-term ground movements associated with closely spaced multiple tunnels [4]. The research about numerical modelling of twin tunnels demonstrated that when the tunnels are positioned at a distance equal to 3.5 times of their radius (3.5r) from one another, the interaction effects between the tunnels become negligible [4]. Furthermore, construction of a new tunnel in close proximity to an already existing tunnel exerts an influence on the latter, resulting in alterations to the magnitudes of forces, bending moments, settlements, and displacements. Meanwhile, the behavior of the newly constructed tunnel is apparently equivalent to that of an individual tunnel [5]. Effects of different stages of construction of intersections on stress distribution and ground deformation was investigated by using finite-element models [6]. Lin conducted a numerical modeling study to investigate the factors influencing the seismic performance of twin tunnels. They specifically examined the performance of the tunnels when subjected to S and P waves. The analysis revealed that the construction of two tunnels in close proximity results in a change in stress distribution due to the interference of the tunnel stress field [7]. In a series of studies, the impact of excavation clearance of the earth pressure balance (EPB) shield on the settlement of existing structures was evaluated. The construction process and monitoring measures in a case study involving the Chongwenmen subway station of Beijing Subway Line 5 excavated below the existing Line 2 were investigated [8,9]. Deformation issues in the strata and nearby structures resulting from the excavation of multi-tunnels were examined, along with various 3D numerical analyses for tunnels at different spacing [10]. Dynamic response and failure characteristics of parallel overlapped tunnels under seismic loadings were assessed using shaking table tests, and the failure mode of the tunnels was analyzed through macroscopic test phenomena [11]. According to the relative relationship of space and structure in the cross tunnel, they were divided into two types: structural cross and spatial cross [11–13]. The structural cross tunnel was divided into structural bifurcation, structural connection channel, and structural wind types; the spatial cross tunnel was divided into spatial orthogonal, spatial parallel, and spatial oblique types, as shown in **Figure 1** [11–13]. Numerical simulations of excavation processes were conducted using the full-section method, step method, and center cross diagram (CRD) method, revealing that construction methods influence the variation degrees of surrounding rock stress, displacement, building deformation, and tunnel convergence [14]. Additionally, the effect of variable depth and in-situ stresses on various angles of tunnel intersections under similar rockmass conditions was assessed through the analysis of thirty-nine cases [15].

With the development and urban expansion, the demand for underground

structures has surged worldwide, particularly in metropolitan areas. In response to this growing need, numerous spatial orthogonal tunnels have been constructed along metro lines in various cities globally. However, despite their significance in enhancing transportation networks and urban connectivity, these underground structures are susceptible to potential risks, particularly during seismic events. The presence of cracks in tunnels and underground structures not only compromises their structural integrity but also can escalate into more severe issues, impacting the overall functionality and longevity of these essential underground facilities [16,17].

As mentioned earlier, studies have been conducted on intersection tunnels, but there is still a gap in comprehensive dynamic studies resulting from the actual application of seismic acceleration and finding the optimal distance between tunnels among studies. Therefore, in this research, with considering four different placement scenarios for two urban metro tunnels, three-dimensional numerical modeling was employed to find the optimal distance between tunnels in a dynamic state. Additionally, in this research, an attempt has been made to use the assumptions of the intersection of lines 6 and 7 of the Tehran metro for a more realistic modeling of spatial orthogonal tunnels.

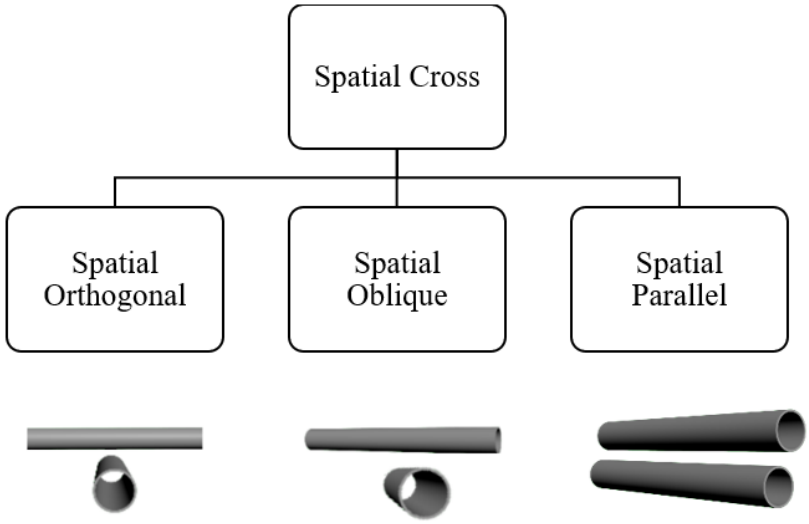

Figure 1. Classification of spatial cross tunnels.

2. Methodology

This study examined four distinct scenarios regarding to the spacing between spatial orthogonal tunnels, and afterwards conducted dynamic analysis in order to determine the most appropriate distance. The ideal spacing between spatial orthogonal tunnels is determined by minimizing their mutual interaction while maintaining efficient operation. According to research conducted by scholars in the field of tunnel engineering, it has been generally observed that in the case of two circular tunnels with identical radius (r) and subjected to hydrostatic stress conditions, the mutual influence or interaction between the tunnels can be ignored when the distance between their centres is six times the radius of each tunnel (6r) [18]. Placing tunnels at very far distances in urban metro lines to avoid the influence of their stress fields is practically not feasible. Firstly, as the depth of the lower tunnel placement increases, the drilling

and stabilization costs significantly rise, and passenger access from the ground surface becomes very difficult. Therefore, tunnels need to be constructed closer to each other. For this purpose, in this study, the effect of tunnel placement at four different depths in a dynamic loading was investigated, and the bending moments, axial forces, and deformations for both tunnels were evaluated in various scenarios of their placement relative to each other. In **Figure 2**, a view of the positioning of the tunnels relative to each other is shown, and in **Table 1**, the different scenarios of their placements are presented respectively.

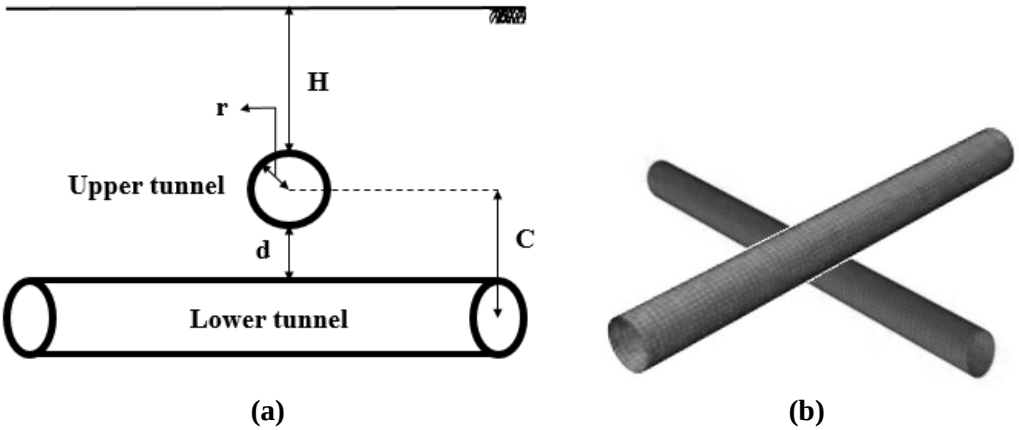

Figure 2. The view of spatial orthogonal tunnels' placement **(a)** 2D view; **(b)** 3D view.

Table 1. Different status of spacing tunnels and their placement.

Scenarios	Distance from the ground (H)	Spacing between tunnels (d)	Centre to centre distance of tunnels (C)
Case 1	14.5 m	0.5r*	2.5r
Case 2	14.5 m	r	3r
Case 3	14.5 m	1.5r	3.5r
Case 4	14.5 m	2r	4r

* In this paper, (r) represents the radius of the tunnels which equals to 4.58 m based on tunnel line 6 and 7 of Tehran metro.

3. Assumptions

3.1. Material properties and constitutive models

In this study, to numerically model and examine the impact of tunnel spacing and the interaction of intersecting tunnels, the geotechnical investigations and reports conducted at the 17 Shahrivar Station (the intersection of Tehran metro lines 6 and 7) were utilized for a more realistic modeling of spatial orthogonal tunnels. In dynamic analysis, the selection of an appropriate constitutive model is crucial for accurately capturing the behavior of soil under varying conditions. Needless to say that, at very small strain levels, the soil exhibits high stiffness, which gradually decreases as the strain increases. It is essential to account for this non-linear variation in stiffness to ensure the accuracy of the analyses. When subjected to dynamic loading, such as earthquake wave propagation, the soil typically experiences small strains. This characteristic makes the small-strain hardening soil behavioral model, like the

HSsmall model, particularly well-suited for dynamic analyses within the PLAXIS software. By considering the nuanced changes in stiffness with strain, the HSsmall model enables a more precise representation of the soil behavior under dynamic conditions. Therefore, in this research, to achieve accurate results the soil surrounding the tunnels was defined using HSsmall constitutive model, whilst the concrete lining of the tunnels was defined using a linear elastic model. Regarding the modeling of the tunnel lining in this study, the effects of segments forming the lining were not evaluated and the tunnel lining is considered homogeneous and constructed at once. The Mechanical properties for the materials utilized are given in **Tables 2** and **3** which are based on geotechnical investigations conducted at the 17 Shahrivar Station of Tehran Metro construction project [19]. The diameters of the tunnels known as line 6 and line 7 Tehran metro are 9.19 m and 9.16 m, respectively. However, for the sake of modelling, both tunnels were assumed to have a diameter of 9.16 m and the thickness of linings for both tunnels are 50 cm.

Table 2. Material properties of the HSsmall model.

Type	Unit weight (kg/m^3)	Cohesion (kPa)	Friction angel (Degree)	E_{50}^{ref} (MPa)	E_{ur}^{ref} (MPa)	G_0^{ref} (MPa)	$\gamma_{0.7}$ ($\times 10^{-3}$)	υ
Soil	1840	18	30	80	240	208	0.15	0.3

Table 3. Material properties of the tunnel lining.

Type	EA (kN/m)	EI (kN·m/m)	d (m)	W (kN/m/m)	υ
Concrete	3.9×10^6	6.1×10^4	0.5	8.4	0.25

3.2. Seismic load

To investigate the dynamic performance of the tunnels under seismic loading, all models and scenarios were analysed using the 7.4 magnitude Tabas earthquake acceleration spectrum which is shown in **Figure 3** [20]. Proper modelling of the boundaries played a crucial role in the study. Special conditions were applied to prevent spurious wave reflections at the model boundaries, which do not occur in reality. Subsequently, a non-linear dynamic analysis based on the hardening soil with small strain constitutive model was conducted using PLAXIS 3D software. The propagation of waves through the soil, considering the Tabas earthquake accelerogram spectrum, and its impact on the tunnel were investigated.

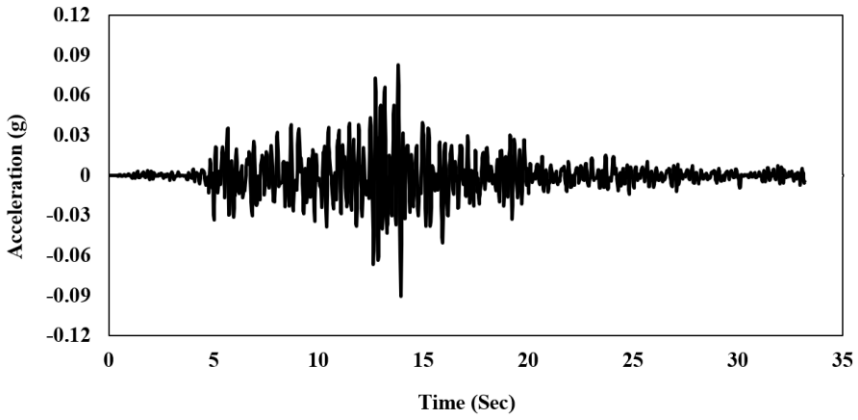

Figure 3. Tabas earthquake accelerogram in the L-direction.

3.3. Mesh properties

Considering the size of the mesh has an important effect on the accuracy of the results in dynamic simulation, Kuhlemeyer and Lysmer [21] suggested the Equation (1). Based on this equation, the mesh dimension in the FEM software must be less than Δl.

$$\Delta l \leq \lambda/10 = Cs/(10f) \quad (1)$$

In this equation, "Δl" represents the maximum acceptable mesh length, "Cs" represents the shear wave velocity, and "f" represents the earthquake frequency. To calculate the dominant frequency of Tabas earthquake acceleration spectrum, Fourier analysis was performed in SeismoSignal software. Fourier analysis transform the signal from the time domain to the frequency domain and the dominant frequency component from the frequency spectrum provided by the software can be identified. This is typically the frequency at which the amplitude of the signal is highest.

The dominant frequency of the Tabas earthquake was 7.14 Hz, and the shear wave velocity was approximately 226 m/s. As a result, the mesh length cannot exceed 3.16 m. The modelling for this work was carried out, with an average mesh length of 2.5 m. **Figure 4** shows the mesh distribution on tunnels. To have a very precise analysis, mesh has been refined in the near area of the tunnels. Furthermore, to ensure that the model's boundaries have no noticeable effect on the results, the distance between the model's boundary and the centre of tunnels must be at least ten times the diameter (10 D) of the tunnels [10]. The dimensions of the model and tunnels' placement are shown in **Figure 4**.

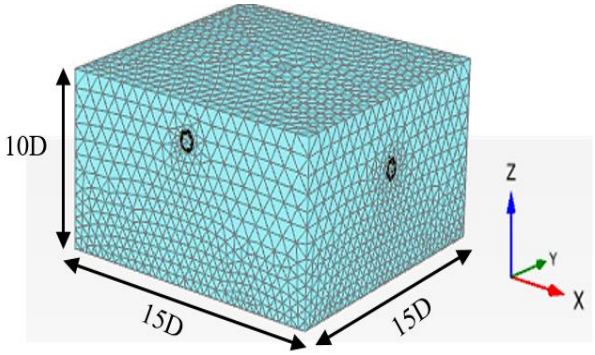

Figure 4. Geometry and mesh generation in numerical modelling.

4. Software validation

In order to validate the performance of the three-dimensional PLAXIS software, the results obtained from numerical modelling in this software were compared with the results from theoretical methods (Penzien and Wu [22], Wang [23] equations) as well as the numerical modelling conducted by Lu et al. They investigated the dynamic performance of circular tunnels under the shear wave propagation using the MIDAS software [24]. **Table 4** presents the soil parameters and concrete lining mechanical properties employed in the modelling [24]. Given that the theoretical solutions are based on a linear elastic constitutive model, it was deemed appropriate to utilize the same linear elastic model for both the soil and tunnel lining in the numerical modelling process. **Figure 5** illustrates the three-dimensional mesh generation and result of the

bending moment in PLAXIS 3D software.

Table 4. Mechanical properties of material in linear elastic constitutive model.

Material type	Specific weight (kN/ m^3)	Poisson's ratio	Elasticity modulus (MPa)
Soil	20	0.25	1.03
Concrete	25	0.25	38

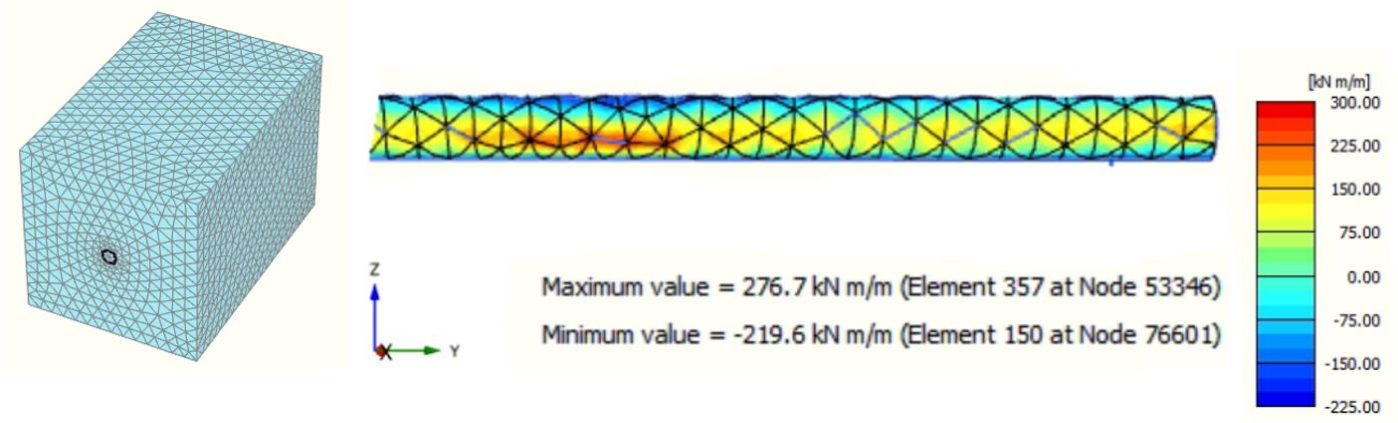

(a) **(b)**

Figure 5. Circular tunnel model in PLAXIS 3D software **(a)** mesh generation; **(b)** bending moment results.

The values of bending moment and axial force using theoretical methods, two-dimensional and three-dimensional MIDAS software, and PLAXIS 3D software are presented in **Table 5**. The results were acquired through the implementation of shear waves on the model. Based on the **Table 5**, it can be concluded that the results of the software programs display a high level of similarity to the outcomes obtained through theoretical equations and other numerical modelling. Consequently, the PLAXIS 3D software holds potential for utilization in this research.

Table 5. Comparison of axial force and bending moment using theoretical methods and numerical modelling.

Parameters	Penzien [22]	Wang [23]	MIDAS 2D [24]	MIDAS 3D [24]	PLAXIS 3D
Axial force (kN)	104.1	2085.4	1985.21	2044.7	2066
Bending moment (kN·m)	260.2	261.5	243.1	272.7	276.7

5. Results and discussion

In this study, the investigation focused on the dynamic seismic loading, specifically examining four distinct distances between spatial orthogonal tunnels, as previously clarified. In the conducted modelling, the upper tunnel is first modelled and its lining is installed, then the lower tunnel is modelled and its supporting system is installed. Finally, under the seismic load of Tabas spectrum, the model is analysed and evaluated. Based on this, the results of bending moment, axial force, and deformations in the tunnels for various static and dynamic conditions are obtained for both tunnels.

5.1. Bending moment results

The variations of the maximum bending moment in tunnels' lining are given in **Figure 6** and the summary of the results presented in **Table 6**. The following figure and table are contained these parameters:

M_U: The maximum static bending moment in the upper tunnel lining prior to the beginning of the lower tunnel construction.

M_{UL}: The maximum static bending moment in the upper tunnel lining subsequent to the completion of the lower tunnel.

M_L: Maximum static bending moment in the lower tunnel lining after its construction.

M_{LD}: Maximum dynamic bending moment in the upper tunnel lining.

M_{UD}: Maximum dynamic bending moment in the lower tunnel lining.

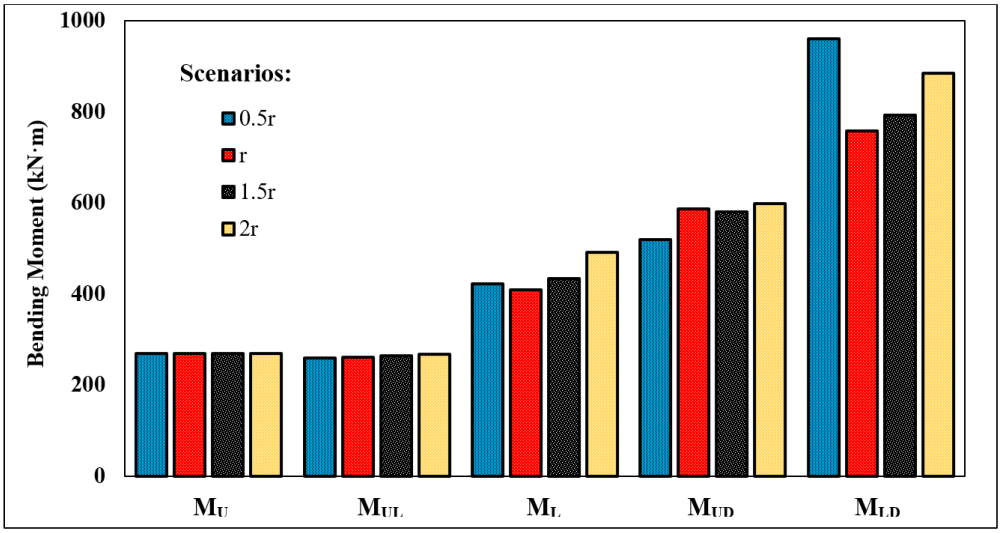

Figure 6. Variations of bending moment induced in tunnels lining in four scenarios of tunnels placement.

Table 6. Summary of the maximum bending moment variations in tunnels.

Scenarios	Spacing between tunnels	M_U (kN·m)	M_{UL} (kN·m)	M_L (kN·m)	M_{UD} (kN·m)	M_{LD} (kN·m)
Case 1	0.5r	268.8	259	421.5	520	959.3
Case 2	r	268.8	261.4	409.7	587.2	757
Case 3	1.5r	268.8	265.1	433.4	579.5	792
Case 4	2r	268.8	267.7	491	598	884

Based on results in the **Figure 6**, the initial static bending moment value in the upper tunnel before the construction of the lower tunnel (M_U) was 268.8 kN·m, and this value had very insignificant changes after the construction of the lower tunnel (M_{UL}), indicating that statically, the lower tunnel in all four placement scenarios has a minimal impact on the upper tunnel. The static results of the bending moment in the lower tunnel (M_L), which are 421, 409, 433, and 491 kN·m for placement scenarios 1 to 4 respectively, show that placing the tunnels in scenario 1 subjects the lower tunnel to the stress field of the upper tunnel, resulting in an increased bending moment. However, in the following scenarios, the trend of increasing the bending moment in

the lower tunnel becomes more reasonable as the tunnels are positioned at a greater distance. This is because with an increase in the depth of placement, the static bending moment also increases on the lower tunnel, making the increase in bending moment more logical.

Dynamic analyses also show similar results to static analysis. Accordingly, the dynamic bending moment values in the upper tunnel in various placement scenarios are 520, 587, 579, and 598 kN·m, and the dynamic bending moment in the lower tunnel is 959, 757, 792, and 884 kN·m respectively. It seems that the lower tunnel absorbs seismic energy by creating local stiffness under the upper tunnel, resulting in lower bending moment in the upper tunnel when the distance between the tunnels is minimized. This issue is clearly evident in the lower tunnel, where a bending moment of approximately 959 kN·m is induced in the lining of the lower tunnel at the closest distance between the two tunnels, which is about 2.27 times the static bending moment itself. Therefore, it is quite clear that placing the tunnels closer than 0.5r causes interference in their stress fields and imposes significant effects on each other.

In order to carry out a comprehensive investigation of the bending moment, axial force, and displacements at the tunnels under different placement configurations, this research focuses on three control points positioned at the upper and lower tunnel intersections. The aforementioned points are illustrated in **Figure 7**. To this purpose, **Figure 8** depicts the variations in bending moment induced at three control points during the Tabas earthquake over time.

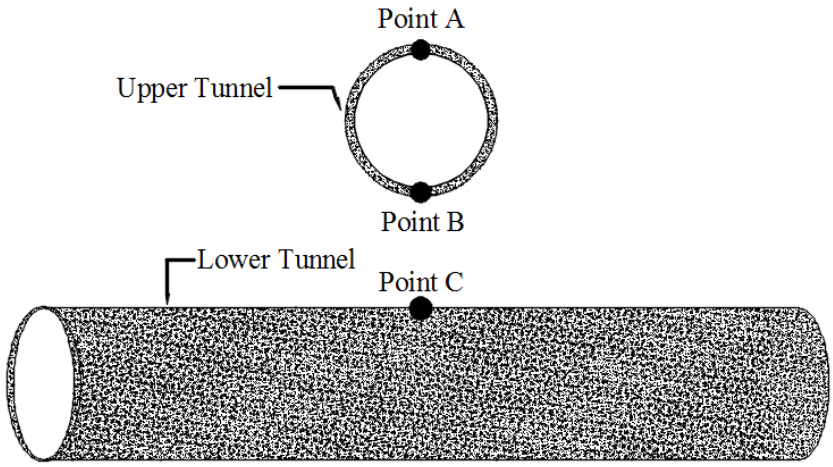

Figure 7. Three control points positioned at the upper and lower tunnels.

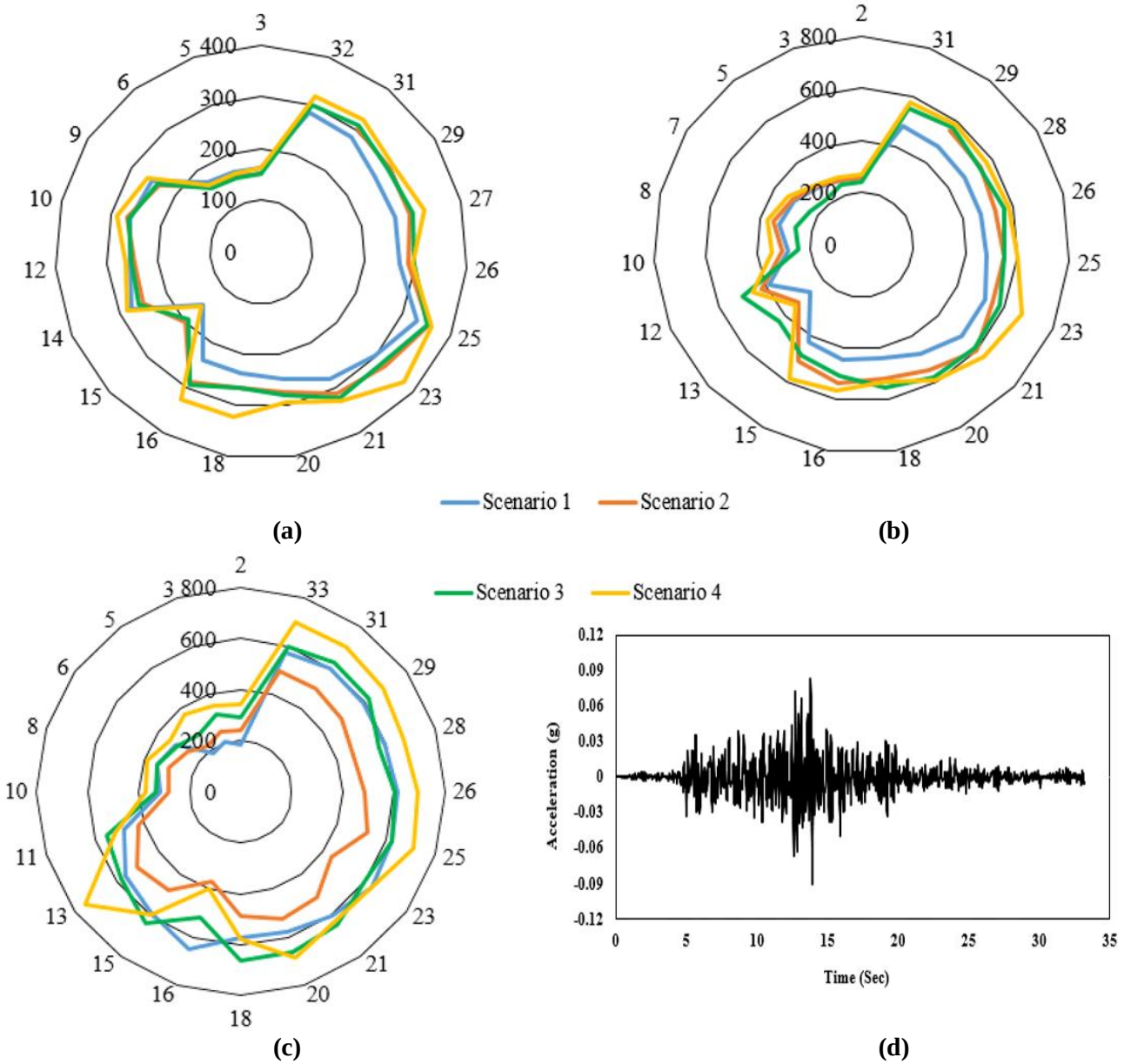

Figure 8. Variation in bending moment induced at three control points during the Tabas earthquake over time: **(a)** point A; **(b)** point B; **(c)** point C; **(d)** tabas earthquake accelerogram.

Figure 8a shows the changes in bending moments that occur in the lining of tunnel control point A (upper tunnel ceiling) relative to the time of dynamic loading from the Tabas earthquake. According to this figure, the considered positioning scenarios for the tunnels have little impact on the bending moments that occur in the upper tunnel ceiling. However, by constructing a tunnel underneath the upper tunnel, localized stiffness is created in the lower part of the upper tunnel which can lead to a reduction in bending moments there. This issue is clearly observable in seconds 14 to 16 of the earthquake. **Figure 8b** also has a very similar trend to **Figure 8a** and shows that the upper tunnel is influenced by localized stiffness resulting from the construction of a tunnel below it, and with increasing distance between the tunnels due to a decrease in localized stiffness in the lower part of the upper tunnel, the bending moment in the dynamical analysis at control point B increases. **Figure 8c** also shows

the changes in bending moments that occur in the lining of the lower tunnel. According to this figure, with the positioning of the tunnels in scenario 1, the lower tunnel is under the influence of the stress field of the upper tunnel and the bending moment in the dynamic analysis increases. However, in scenario 2, it is evident that the tunnels are out of each other's influence zone and do not have a negative effect on each other. It can also be said that in scenarios 3 and 4, with an increase in the depth of the lower tunnel, more overburden and soil pressure are exerted on the lower tunnels leading to an increase in bending moment in them. It can be argued that scenario 2, while imposing less overburden on the lower tunnel, creates an appropriate distance between the two tunnels, preventing them from being under each other's influence, so that it can be an optimal scenario for the placement of tunnels.

5.2. Axial force results

Concrete lining is designed based on the bending moment and axial force induced on the tunnels in static and dynamic conditions. Hence, the axial force amount in the tunnel's lining can be an important criteria in tunnel design. Consequently, in this research the axial force induced in the tunnels linings for different scenarios of tunnels placement were investigated. In this regard, the variations of the maximum axial force in tunnels' lining are evaluated based on the results illustrated in **Figure 9** and the summary of the results presented in **Table 7**. The following figure and table are contained these parameters:

P_U: Maximum static axial force in the upper tunnel lining before the construction of the lower tunnel.

P_{UL}: Maximum static axial force in the upper tunnel lining after the construction of the lower tunnel.

P_L: Maximum static axial force in the lower tunnel lining after its construction.

P_{UD}: Maximum dynamic axial force in the upper tunnel lining.

P_{LD}: Maximum dynamic axial force in the lower tunnel lining.

According to the **Figure 9** and **Table 7**, the maximum axial force value in the lining of the upper tunnel before the construction of the lower tunnel (P_U) is 410 kN, which then increases to 696.2, 475.5, 425.1, and 420.6 kN in different scenarios of the lower tunnel placement (P_{UL}). In fact, the construction of the lower tunnel introduces local stiffness around the upper tunnel, leading to an increase in the axial force in its lining. Additionally, the axial force in the lower tunnel (P_L) indicates that with an increase in the depth of tunnel placement, the superimposed load also increases, resulting in an increase in the axial force induced in it. However, in the dynamic state, the increase in axial force in the upper tunnel is much higher than in the static state. This is because with an increase in local stiffness in the surrounding of the upper tunnel, the absorption of seismic energy in it increases, and the dynamic axial force significantly rises. Therefore, the dynamic axial force in the upper tunnel increases approximately 3.4 times when the distance between the tunnels is less than 0.5r (scenario 1), indicating the impact of tunnel spacing and their interaction on each other. Neglecting this issue may lead to unforeseen forces exceeding limits in tunnels during an earthquake, resulting in instability, collapse, and the formation of cracks in tunnels and underground spaces.

Based on **Tables 6** and **7**, it can be concluded that the placement of tunnels in scenario 2) can be considered as an optimal condition because the results show that placing the tunnels in this condition makes them less affected by their stress fields. It is essential to note that in urban tunnels, the deeper the tunnel placement, the higher the construction costs and the difficulty in passenger access from the ground surface, leading to challenges. Therefore, the optimal distance between two tunnels is when they have less impact on each other and the depth of the lower tunnel is within a suitable range, both of which are present in placement scenario 2.

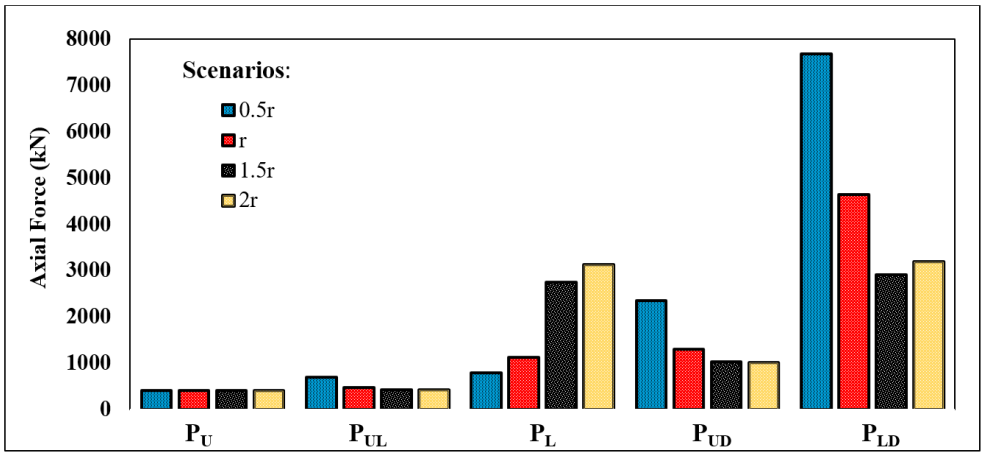

Figure 9. Variations of axial force induced in tunnels lining in four scenarios of tunnels placement.

Table 7. Summary of the axial force variations in tunnels.

Scenarios	Spacing between tunnels	P_U (kN)	P_{UL} (kN)	P_L (kN)	P_{UD} (kN)	P_{LD} (kN)
Case 1	0.5r	410.3	696.2	785	2353	7689
Case 2	r	410.3	475.5	1126	1293	4638
Case 3	1.5r	410.3	425.1	2749	1033	2908
Case 4	2r	410.3	420.6	3127	1005	3195

In structural internal force analysis, besides stating the magnitude of the values, the distribution of these values can be very important. Hence, to this purpose, **Figure 10** shows the variations in axial force induced at three control points (**Figure 7**) during the Tabas earthquake over time.

Based on **Figure 10a**, in order to compare the variation of axial force induced in tunnel lining for four tunnels' placement scenarios, it can be noted that in dynamic analysis, placing tunnels within less than half of their radius (<0.5r) can directly impact the above tunnel and affect its stress field, which is clearly observed during seconds 10 to 15 of the earthquake. Additionally, increasing the distance between tunnels reduces their impact on each other, so that the axial in the ceiling of the upper tunnel in cases 3 and 4 is almost the same. According to **Figure 10b**, during the peak acceleration of the earthquake, the effects of tunnels in scenarios 1 and 2 are distinct and clear, causing changes in the stress field of the tunnels and resulting in changes in the magnitude and direction of the bending moment in the floor of the upper tunnel. These sudden changes in bending moment amount and direction may sometimes lead

to local instabilities in the tunnel lining. Furthermore, based on **Figure 10c**, the axial force induced in the ceiling of the underlying tunnel increases with the distance between tunnels, which is due to the increased depth of tunnel placement and their overburden. However, it is clear in this figure that placement scenario case 1 (<0.5r), results in a sudden and severe axial force in dynamic loading at point C, which may lead to instability in this underlying tunnel.

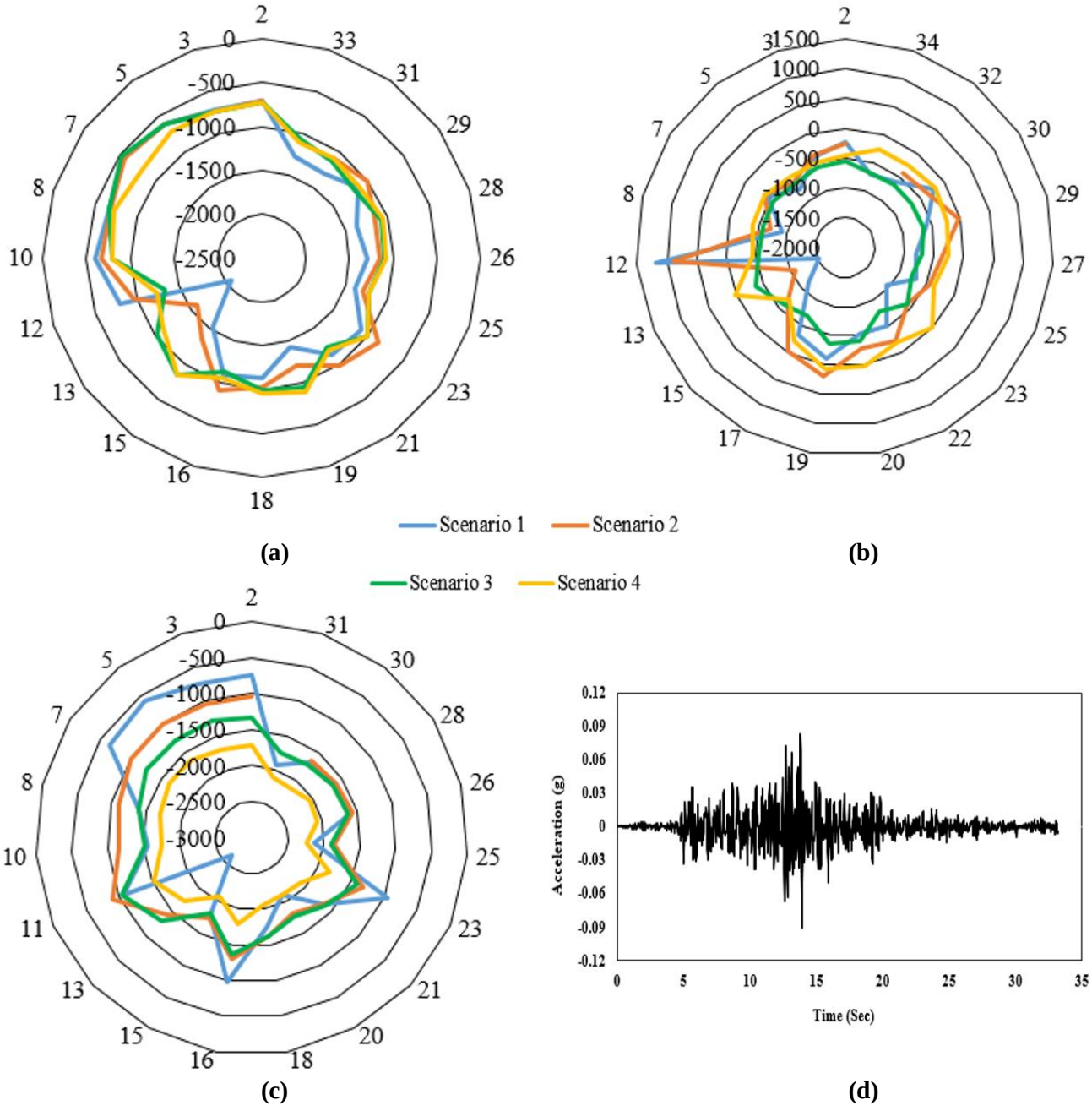

Figure 10. Variation in axial force induced at three control points during the Tabas earthquake over time: **(a)** point A; **(b)** point B; **(c)** point C; **(d)** tabas earthquake accelerogram.

5.3. Displacement results

Figure 11 and **Table 8** present the observed changes in the maximum displacement along the Z-axis at the point of intersection between the tunnels for

different tunnel placements. The following figure and table are contained these parameters:

Z_U: Maximum static displacement in the Z-axis direction in the upper tunnel lining before the construction of the lower tunnel.

Z_{UL}: Maximum static displacement in the Z-axis direction in the upper tunnel lining after the construction of the lower tunnel.

Z_L: Maximum static displacement in the Z-axis direction in the lower tunnel lining after its construction.

Z_{UD}: Maximum dynamic displacement in the Z-axis direction in the upper tunnel lining.

Z_{LD}: Maximum dynamic displacement in the Z-axis direction in the lower tunnel lining.

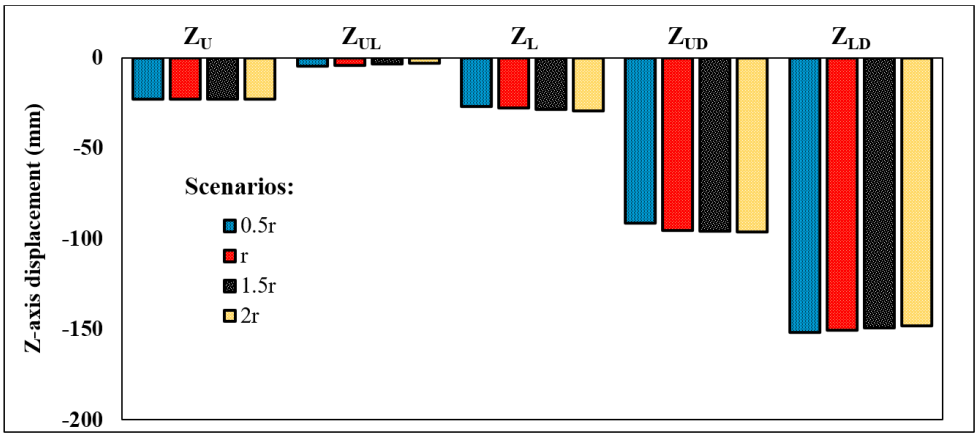

Figure 11. Variations of displacement in the Z-axis in tunnels in four scenarios of tunnels placement.

Table 8. Summary of displacement in the Z-axis in tunnels.

Scenarios	Spacing between tunnels	Z_U (mm)	Z_{UL} (mm)	Z_L (mm)	Z_{UD} (mm)	Z_{LD} (mm)
Case 1	0.5r	−22.85	−4.81	−26.77	−91.5	−151.9
Case 2	r	−22.85	−4.087	−27.57	−95.51	−150.6
Case 3	1.5r	−22.85	−3.427	−28.48	−95.62	−149.2
Case 4	2r	−22.85	−2.89	−29.58	−96.1	−148

The results obtained from numerical modelling in **Figure 11** and **Table 8** show that the distance between tunnels has little influence on the vertical displacement of the tunnels both statically and dynamically. It seems that the distance between tunnels only affects the bending moment and axial force in the lining by changing the stress fields in them and has a lower impact on displacements. Additionally, according to the results of **Table 8**, it can be inferred that in the event of an earthquake, significant displacements occur in the tunnels compared to their static state. In static conditions, the vertical deformation of the upper tunnel is around 4 mm, but under seismic loading, this deformation reaches about 90 mm. Similarly, for the lower tunnel, static deformation of about 26 mm increases to approximately 150 mm under seismic loading.

For further investigation of the effect of tunnels constructed adjacent to each

other, the displacements at three control points referenced in **Figure 7** were studied under dynamic loading conditions, as shown in **Figure 12**, which displays the displacements in the Z-axis direction for these three points and with consideration of four tunnel positioning scenarios (**Table 1**), relative to the time of dynamic loading. According to **Figure 12a**, the distance between the tunnels does not have a significant impact on the displacements occurring in the upper tunnel ceiling. However, in **Figure 12b**, it can be observed that due to the localized stiffness resulting from the construction of the lower tunnel beneath the upper tunnel, in scenarios 1 to 3, the displacements in the upper tunnel floor are almost the same, but with an increase in the depth of the lower tunnel and a decrease in relative localized stiffness, the displacement at point B increases and its direction oscillates noticeably. **Figure 12c** clearly shows the effect of the distance between the tunnels on the displacements occurring in the lower tunnel. According to this figure, in positioning scenario 1, the tunnels have the greatest impact on each other and cause the maximum displacement at control point C. Consequently, based on **Figures 8**, **10** and **12**, it can be stated that by placing the tunnels in scenario 1 (with the distance between the tunnels less than half of their radius), the tunnels have a significant impact on each other, leading to an increase in internal forces and displacements in the tunnel lining under dynamic conditions, which can result in localized instability in part of the tunnel lining and cause damage to underground structures.

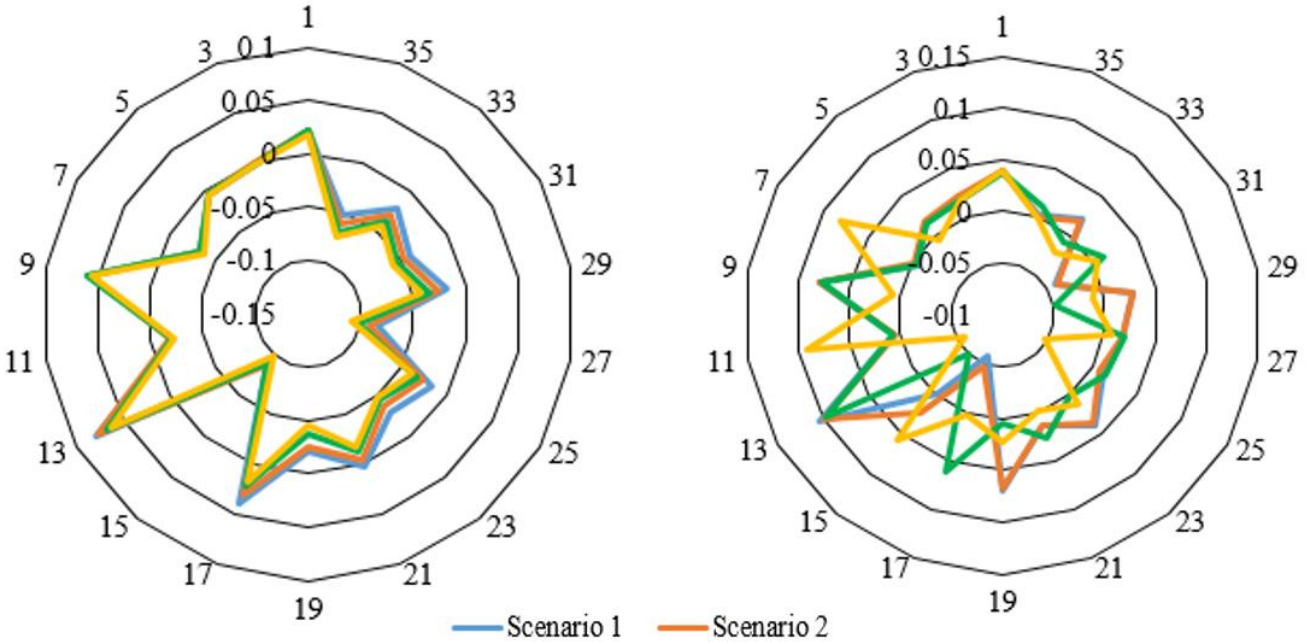

(a) **(b)**

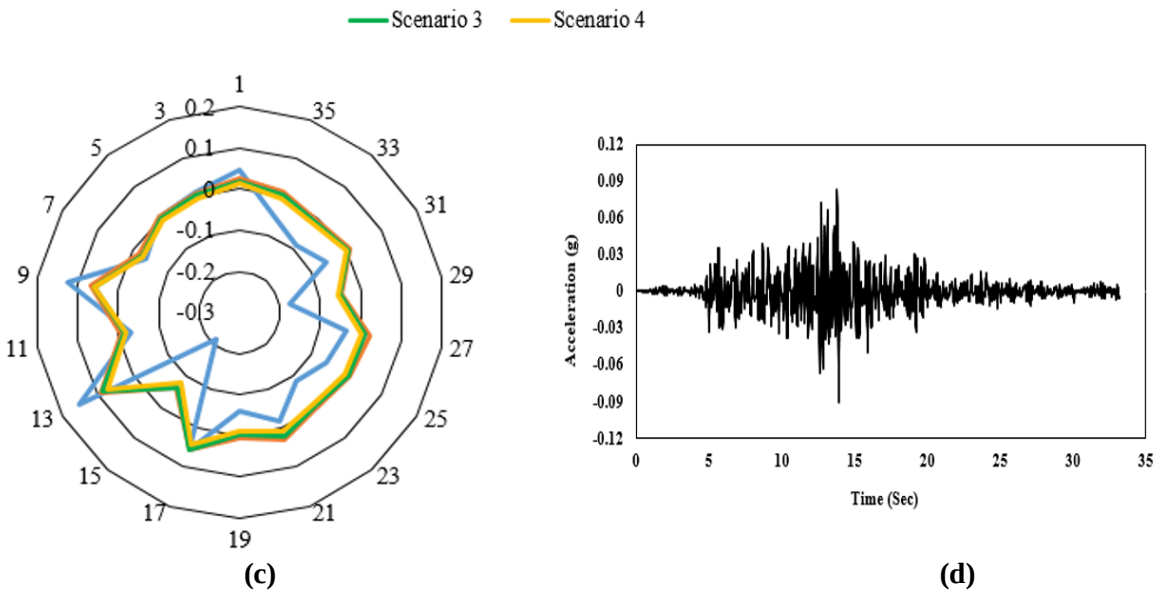

(c) **(d)**

Figure 12. Variation in displacement induced at three control points during the Tabas earthquake over time: **(a)** point A; **(b)** point B; **(c)** point C; **(d)** tabas earthquake accelerogram.

5.4. Plastic points

Figures 13–17 depict the plastic points that were formed within the model during both dynamic and static studies under the scenario 2. The number of plastic points in the vicinity of the tunnels starts out small following their construction. However, subsequent to the construct of the lower tunnel, there is an observed increase in the concentration of plastic particles within the space between the two tunnels. The dynamic loading exerted on the surrounding soil, which yields the soil in some points and results in displacements and deformations in tunnel lining. During the phase of dynamic analysis, it is observed that there is an increase in yielding in the vicinity of the ground surface over time. It is important to acknowledge that the plastic points refer to the soil surrounding the tunnel. As depicted in **Figure 17**, the tunnel lining does not exhibit any yielding or plastic points when subjected to both static and dynamic conditions which indicates that tunnels placement in scenario 2 can be an effective and appropriate placement of tunnels.

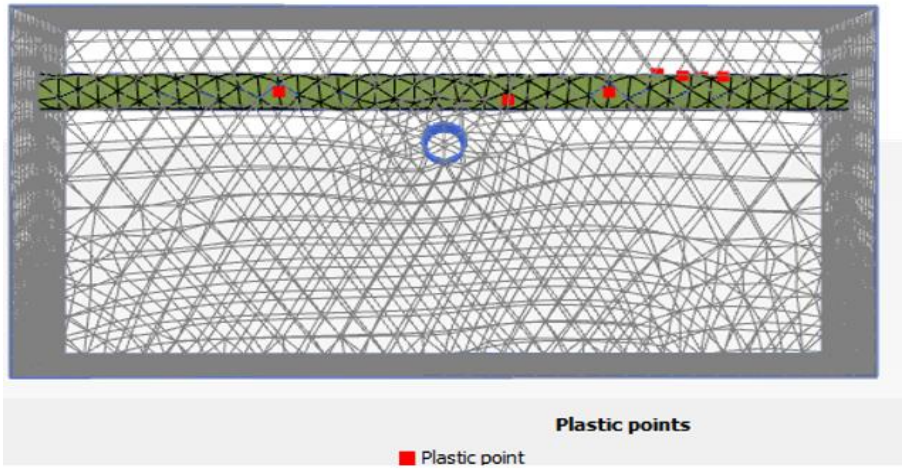

Figure 13. Plastic points formed in model after the construction of upper tunnel.

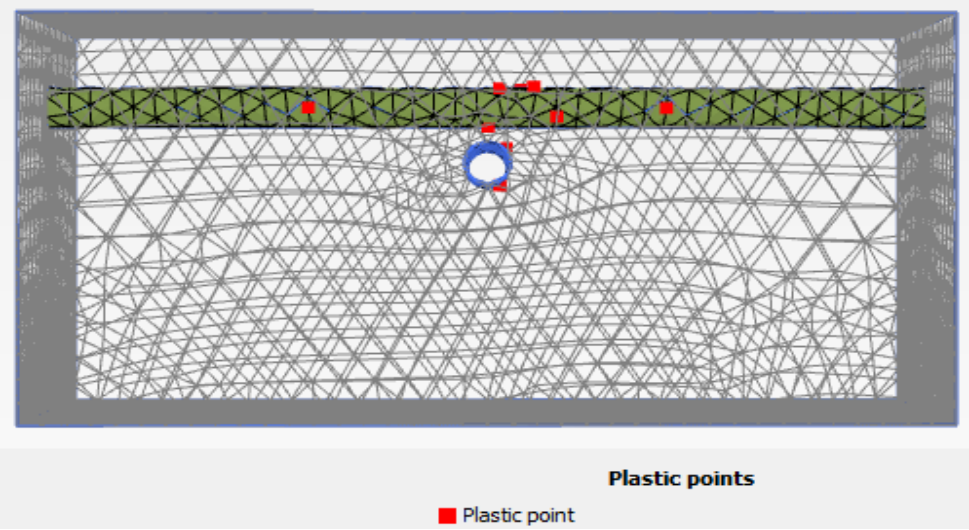

Figure 14. Plastic points formed in model after the construction of lower tunnel.

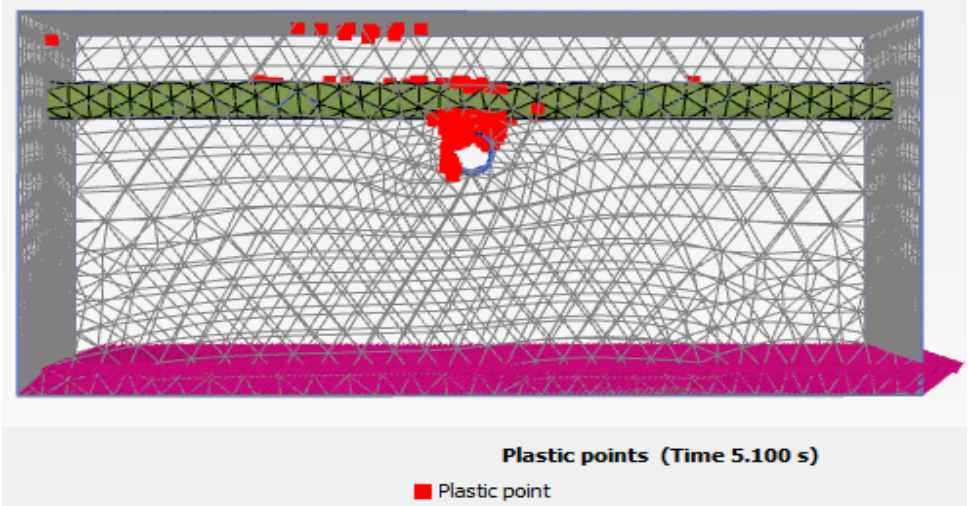

Figure 15. Plastic points formed in model in the time of 5.1s in dynamic analysis.

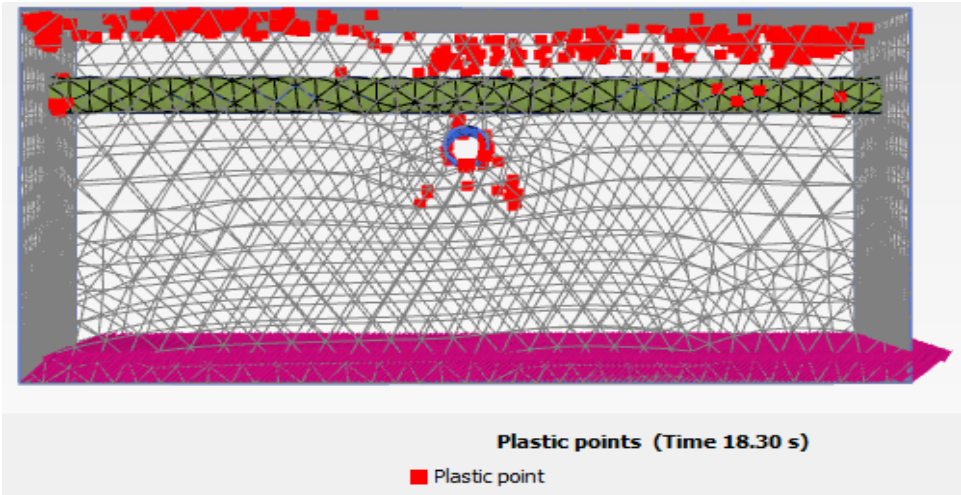

Figure 16. Plastic points formed in model in the time of 18.3s in dynamic analysis.

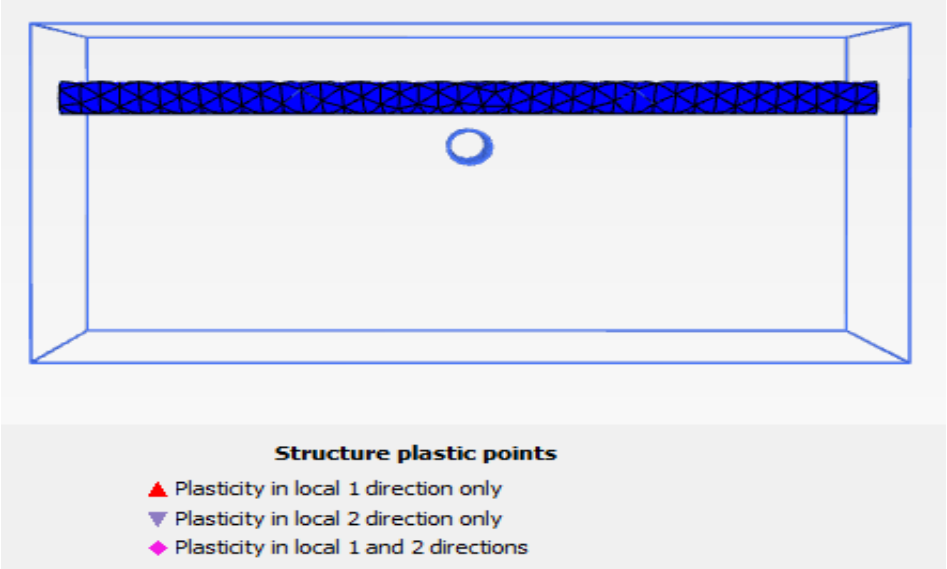

Figure 17. Plastic points in tunnel lining for scenario 1.

6. Conclusion

This study examined four distinct scenarios regarding to the spacing between spatial orthogonal tunnels, and afterwards conducted dynamic studies in order to determine the most appropriate distance. The ideal spacing between spatial orthogonal tunnels is determined by minimizing their mutual interaction while maintaining efficient operation. According to results of dynamic FEM analysis, the following general conclusions can be drawn from this study:

1) Placing the tunnels in scenario 1 (<0.5r) subjects the lower tunnel to the stress field of the upper tunnel, resulting in an increased bending moment. However, in the following scenarios, the trend of bending moment variations in the lower and upper tunnels become more reasonable as the tunnels are positioned at a greater distance.
2) In dynamic analyses it seems that the lower tunnel absorbs seismic energy by creating local stiffness under the upper tunnel, resulting in lower bending moment in the upper tunnel when the distance between the tunnels is minimized (for distances less than 0.5r).
3) In the lower tunnel, dynamic bending moment is approximately 2.27 times the static bending moment itself. Therefore, it is quite clear that placing the tunnels closer than 0.5r (<0.5r) causes interference in their stress fields and imposes significant effects on each other.
4) In scenario 1, when the distance of tunnels is less than 0.5r (<0.5r), due to the increasing the local stiffness in the surrounding of the upper tunnel, the dynamic axial force in the upper tunnel increases approximately 3.4 times the static axial force, indicating the impact of tunnel spacing and their interaction on each other.
5) The distance between tunnels has little influence on the vertical displacement of the tunnels both statically and dynamically. However, in positioning scenario 1, the tunnels have the greatest impact on each other and causes the maximum displacement in lower tunnel.
6) The results of the internal forces and displacements in both tunnels under

dynamic loading show that positioning scenario 2 of the tunnels is the most suitable option. Because in this scenario (compared to scenario 1), the tunnels are less affected by each other's stress field, and also in this positioning scenario (compared to scenarios 3 and 4), access from the ground surface to the lower tunnel will be easier and with lower construction costs.

Author contributions: Conceptualization, MM and TAM; methodology, MM; software, MM and SAM; validation, TAM; formal analysis, MM, TAM and SAM; investigation, MM; resources, MM and TAM; data curation, TAM and SAM; writing—original draft preparation, MM and SAM; writing—review and editing, TAM and SAM; visualization, SAM; supervision, MM and TAM; project administration, MM. All authors have read and agreed to the published version of the manuscript.

Conflict of interest: The authors declare no conflict of interest.

References

1. Mohammadifar M, Asheghi T, Fahimifar A. Parametric and Sensitivity Analysis on the Effects of Geotechnical Parameters on Tunnel Lining in Soil Surrounding. Journal of Structural and Construction Engineering (JSCE). 2024. doi: 10.22065/jsce.2024.422469.3250
2. Mehmandari TA. Experimental and numerical analysis of tunnel primary support using recycled, and hybrid fiber reinforced shotcrete. In: Structures. Elsevier. 2024.
3. Kim S. Model testing and analysis of interaction between tunnels in clay. University of Oxford; 1996.
4. Hunt D. Investigating ground movements caused by the construction of multiple tunnels in soft ground using laboratory model tests. Canadian Geotechnical Journal. 2007.
5. Asheghi Mehmandari T, Mohammadi D, Ahmadi M, et al. Fracture mechanism and ductility performances of fiber reinforced shotcrete under flexural loading insights from digital image correlation (DIC). Insight - Civil Engineering, doi: https://doi.org/10.18282/ice.v7i1.611.
6. Golshani A, Joneidi M, Majidian S. 3D numerical modeling for construction of tunnels intersections- case study of Hakim tunnel. Japanese Geotechnical Society Special Publication. 2015; 2(43): 1523-1527.
7. Lin SY, Yang J, Hung HH. Seismic Analysis of twin Tunnels by a Finite/Infinite Element Approach. International Journal of Geomechanics. 2017.
8. Yin M, Jiang H, Jiang Y, et al. Effect of the excavation clearance of an under-crossing shield tunnel on existing shield tunnels. Tunnelling and Underground Space Technology. 2018; 78: 245-258. doi: 10.1016/j.tust.2018.04.034
9. Zhang C, Zhang X, Fang Q. Behaviors of existing twin subway tunnels due to new subway station excavation below in close vicinity. Tunnelling and Underground Space Technology. 2018; 81: 121-128. doi: 10.1016/j.tust.2018.07.020
10. Jin YF, Zhu BQ, Yin ZY, et al. Three-dimensional numerical analysis of the interaction of two crossing tunnels in soft clay. Underground Space. 2019; 4(4): 310-327. doi: 10.1016/j.undsp.2019.04.002
11. Yang T, Rao Y, Wu H, Zhang J. Dynamic Response of Parallel Overlapped Tunnel under Seismic Loading by Shaking Table Tests. Shock and Vibration. 2021; 2021: 2535762.
12. Li P, Lei M. Research progress in the design and construction technology of crossing tunnels. Journal of Railway Science and Engineering. 2014; 11(1): 67-73.
13. Asheghi Mehmandari T. Engineering Concept and Construction Methods of High-Rise Building. Iran: Sanei; 2023. 308p.
14. Ren Y, Zhou S, Jia J, et al. The Influence of Construction Methods on the Stability of Tunnels and Ground Structures in the Construction of Urban Intersection Tunnels. Sustainability. 2023; 15(20): 14720. doi: 10.3390/su152014720
15. Naseri A, Maleki B, Asheghi Mehmandari T, et al. Investigating the Influence of Sample Geometric Variations on Mechanical Characterization in Rock and Concrete. 2024. doi:10.22044/jme.2024.14631.2759

16. Asheghi Mehmandari T, fahimifar A, Asemi F. The Effect of the Crack Initiation and Propagation on the P-Wave Velocity of Limestone and Plaster Subjected to Compressive Loading. AUT Journal of Civil Engineering. 2020; 4(1): 55-62. doi: 10.22060/ajce.2019.15984.5558
17. Zare P, Asheghi T, Fahimifar A, Zabetian S. Experimental Assessment of Damage and Crack Propagation Mechanism in Heterogeneous Rocks. In: 5th International Conference on Applied Research in Science and Engineering. University of Amsterdam, Netherlands. 2020.
18. Brady BH, Brown ET. Rock Mechanics for underground mining, 3rd ed. Kluwer Academic Publisher; 2004.
19. Shirizadeh H, Dehghan S. Determination of the optimal distance of non-planar cross tunnels using numerical method –A case study of the intersection of Tehran Metro Lines 6 and 7. Journal of Tunneling and Underground Space. 2017. doi: 10.22044/tuse.2017.4585.1274
20. Pacific Earthquake Engineering Research Center (PEER) ground motion database. Available online: https://ngawest2.berkeley.edu (accessed on 31 December 2023).
21. Kuhlemeyer RL, Lysmer J. Finite Element Method Accuracy for Wave Propagation Problems. Journal of the Soil Mechanics and Foundations Division. 1973; 99(5): 421-427. doi: 10.1061/jsfeaq.0001885
22. Penzien J, Wu CL. Stresses in linings of bored tunnels. International Journal of Earthquake Engineering and Structural Dynamics. 1998; 7: 283-300. doi: 10.1002/(SICI)1096-9845(199803)27:3<283::AID-EQE732>3.0.CO;2-T
23. Wang JN. Seismic Design of Tunnels: A State-of-the-art Approach. Parsons Brinckerhoff Quade & Douglas, Inc; 1993.
24. Lu Q, Chen S, Chang Y, et al. Comparison between Numerical and Analytical Analysis of the Dynamic Behavior of Circular Tunnels. Earth Sciences Research Journal. 2018; 22(2): 119-128. doi: 10.15446/esrj.v22n2.72248